

Local moment dynamics and screening effects in doped charge-transfer insulators

A. Amaricci,¹ N. Parragh,² M. Capone,¹ and G. Sangiovanni²

¹*Democritos National Simulation Center, Consiglio Nazionale delle Ricerche,
Istituto Officina dei Materiali (IOM) and Scuola Internazionale Superiore
di Studi Avanzati (SISSA), Via Bonomea 265, 34136 Trieste, Italy*

²*Institute for Theoretical Physics and Astrophysics,
University of Würzburg, D-97074 Würzburg, Germany*

(Dated: December 9, 2021)

By means of Dynamical Mean-Field Theory we investigate the spin response function of a model for correlated materials with d - or f -electrons hybridized with more delocalized ligand orbitals. We point out the existence of two different processes responsible for the dynamical screening of local moments of the correlated electrons. Studying the local spin susceptibility we identify the contribution of the “direct” magnetic exchange and of an “indirect” one mediated by the itinerant uncorrelated orbitals. In addition, we characterize the nature of the dynamical screening processes in terms of different classes of diagrams in the hybridization-expansion contributing to the density-matrix. Our analysis suggests possible ways of estimating the relative importance of these two classes of screening processes in realistic calculations for correlated materials.

PACS numbers: 71.27.+a, 71.10.Fd, 71.30.+h

I. INTRODUCTION

The physics of strongly correlated systems can be identified with the process that turns delocalized electrons into localized magnetic moments. In d - and f -electron materials, such as transition-metal oxides (TMO) and heavy fermions (HF), the confined nature of the correlated orbitals gives rise to large spin moments localized over short time scales at each lattice site. In the atomic limit, in which the system is described as a collection of disconnected atoms, such local spins assume the largest value allowed by the atomic configuration, and show no dynamics. On the other hand, in the presence of a fraction of itinerant electrons (*i.e.* away from the extreme case of the atomic limit), the instantaneous value of the local spins gets reduced and a dynamics emerges as an effect of the screening processes.

In TMO sizeable local magnetic moments from d -orbital electrons have been revealed by inelastic neutron scattering (INS) and X-ray absorption spectroscopy (RIXS)¹ in materials like, *e.g.* high- T_c cuprates^{2,3}, cobaltate^{4,5} and iron-based superconductors⁶⁻⁸. The fingerprints of the individual screening processes are hard to extract from the instantaneous value of the local moments. For instance, only indirect information about the nature of the screening of the local moments can be gained from the temperature dependence of the local spin susceptibility^{9,10}. The spin dynamics can instead be a much more sensitive tool to diagnose the physical effects of such screening processes^{11,12}.

From a general point of view one expects two processes to be responsible for the screening of the local moments: *i*) processes involving a *direct* hopping between correlated electrons, and *ii*) processes involving the *hybridization* with more itinerant, *e.g.* ligand p -, orbitals. In the oxides, one associates processes of type *i*) with the super-

exchange mechanism which is captured by a Hubbard-like description including only correlated d -orbitals. This “ d -only” description is good whenever the d -manifold is very well isolated from the ligand p -bands. Processes of type *ii*) can instead be viewed as an additional screening channel, active if the system can gain delocalization energy upon hybridizing with the bath of itinerant electrons.

In the present paper we study the local moment dynamics and the screening effects addressing questions such as: “how can we distinguish between type-*i*) and type-*ii*) contributions to local spin susceptibility?”, or “which features would we expect to see in a INS or RIXS experiment if the screening is dominated by hybridization processes?” In order to do this we focus our attention on doped “charge-transfer” insulators¹³ (CTI), *e.g.* Cuprates, as a paradigmatic example of Mott systems in which the effects of the hybridization are crucial.

We therefore consider a generic, yet simple, model for a CTI in which the doping and the relative importance between the two screening channels can be easily tuned. By using Dynamical Mean-Field Theory (DMFT)¹⁴ we study the local dynamical spin response function. We point out the existence of two distinct features in the local spin susceptibility associated to processes of the two different types and we numerically characterize their nature in a clear way in terms of different classes of diagrams contributing to the density-matrix.

The structure of the paper is as follow: in Sec. II we introduce the theoretical model and briefly discuss its numerical solutions within DMFT. In Sec. III we discuss the results for the local moment dynamics. In Sec. IV we characterize the different features in the spin susceptibility in terms of distinct class of diagrams in the strong-coupling expansion. Finally, section V contains concluding remarks.

II. MODEL

We consider a generalized periodic Anderson model (t_{dd} -PAM)¹⁵ describing a wide-band of conduction electrons, hybridizing with a narrow-band of strongly interacting electrons:

$$H = \sum_{\mathbf{k}\sigma} \varepsilon_p(\mathbf{k}) p_{\mathbf{k}\sigma}^\dagger p_{\mathbf{k}\sigma} + \sum_{\mathbf{k}\sigma} \varepsilon_d(\mathbf{k}) d_{\mathbf{k}\sigma}^\dagger d_{\mathbf{k}\sigma} + t_{pd} \sum_{i\sigma} (d_{i\sigma}^\dagger p_{i\sigma} + p_{i\sigma}^\dagger d_{i\sigma}) + U \sum_i d_{i\uparrow}^\dagger d_{i\downarrow}^\dagger d_{i\uparrow} d_{i\downarrow} \quad (1)$$

The operators $p_{i\sigma}$ ($p_{i\sigma}^\dagger$) destruct (create) electrons in the conduction band with spin- σ with dispersion $\varepsilon_p(\mathbf{k}) = \varepsilon_p - 2t_{pp}[\cos(k_x) + \cos(k_y)]$. Similarly, $d_{i\sigma}$ ($d_{i\sigma}^\dagger$) destruct (create) electrons in the narrow-band with spin- σ and dispersion $\varepsilon_d(\mathbf{k}) = \varepsilon_d - 2\alpha t_{pp}[\cos(k_x) + \cos(k_y)]$, where $\alpha \in [0, 1)$ denotes the bandwidth ratio. The two orbital electrons hybridize with a local amplitude t_{pd} . The last term in Hamiltonian (1) indicates the strong local Coulomb interaction U experienced by the d -electrons.

In the following, we fix the energy unit to the half-bandwidth of the conduction electrons $D = 4t_{pp} = 1$. In addition we shall set the bandwidth ratio to $\alpha = 0.25$ and $\varepsilon_d = 0$. The energy separation between the centers of the two bands $\Delta = \varepsilon_p - \varepsilon_d$ denotes the charge-transfer energy. Finally, we will drop any reference to the spin index, as we focus on the paramagnetic state, where the local moments are not ordered.

The model Hamiltonian (1) interpolates between the Hubbard model (HM) for the correlated d -electrons ($t_{pd} = 0$, $\alpha \neq 0$), and the more usual periodic Anderson model ($\alpha = 0$, $t_{pd} \neq 0$), describing non-dispersive correlated electrons hybridized with a wide-band^{16–19}.

We solve the t_{dd} -PAM using Dynamical Mean Field Theory (DMFT)¹⁴. The DMFT allows us to study the local screening and the spin dynamics in a fully non-perturbative way. Within DMFT, the lattice model (1) is mapped onto an effective impurity problem for a single d -orbital, supplemented by a self-consistency condition for the local *Weiss Field* (WF). The WF \mathcal{G}_{0dd}^{-1} is calculated by isolating the dd -element of the interacting local Green's function, as in general DMFT schemes with enlarged basis-sets^{20–23}. We solve the associated effective impurity problem using exact-diagonalization (ED)^{24–26} and hybridization-expansion continuous-time quantum Monte Carlo (CTQMC) methods^{27–30}.

Within ED the local WF must be represented in terms of a discretized hybridization function: $\Delta_{dd}(i\omega_n) = \sum_{l=1}^{N_b} V_l^2 / (i\omega_n - \varepsilon_l)$ using N_b auxiliary energy levels. The parameters ε_l and V_l describe, respectively, the local energy and the hybridization between the impurity and the l^{th} bath level. All the ED calculations are performed using $N_b = 6$.

The spin susceptibility χ_{spin} is defined as the imaginary part of the dynamical response function:

$$\chi_{\text{spin}}(\omega) = i \int dt e^{i\omega t} \theta(t) \langle [\hat{S}_z^{(d)}(t), \hat{S}_z^{(d)}(0)] \rangle \quad (2)$$

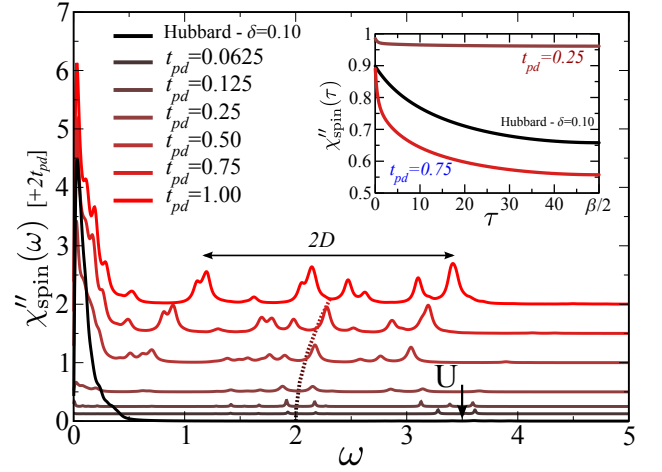


Figure 1. (Color online) Spin susceptibility $\chi''_{\text{spin}}(\omega)$ on the real-axis for increasing values of t_{pd} . The different curves are shifted along the y -axis by $2t_{pd}$ for better comparison. Data are for doping value $\delta = 0.10$. Dotted line is the shift in the position of the p -band from increasing hybridized band repulsion. Inset: imaginary-time spin susceptibility $\chi''_{\text{spin}}(\tau)$ for a fixed doping $\delta = 0.10$ for $t_{pd} = 0.25$ and 0.75 . The black curve corresponds to the Hubbard model result with doping $\delta = 0.10$.

where $\hat{S}_z^{(d)}$ is the z -component of the spin operator on the d -site and $[\cdot, \cdot]$ denotes the commutator. In ED the spin susceptibility is evaluated using the spectral decomposition:

$$\chi''_{\text{spin}}(\omega) = \frac{\pi}{\mathcal{Z}} \sum_{i,j} |\langle i | \hat{S}_z^{(d)} | j \rangle|^2 (e^{-\beta E_j} + e^{-\beta E_i}) \delta(\omega - (E_i - E_j)), \quad (3)$$

where \mathcal{Z} is the partition function.

The hybridization-expansion CTQMC method provides a (statistically) exact solution of the DMFT equations. Indeed, we tested the agreement between ED and CTQMC calculations finding very satisfactory results for both local and dynamical quantities. As we will show, CTQMC permits to investigate the diagrams contributing to the local screening processes. Since this is done using a (infinite series) perturbation-expansion language, it turns out to give useful information about the physics involved in the screening of the local moment.

III. SPIN SUSCEPTIBILITY

As discussed in the Introduction, we focus on doped CTI. By definition this means that the hole doping involves mainly the p -band. This marks a strong difference with a description of pure d -electrons, where the insulator has a Mott-Hubbard character. In order to study the differences in the spin susceptibility and in other observables induced by the hybridization t_{pd} , we want to

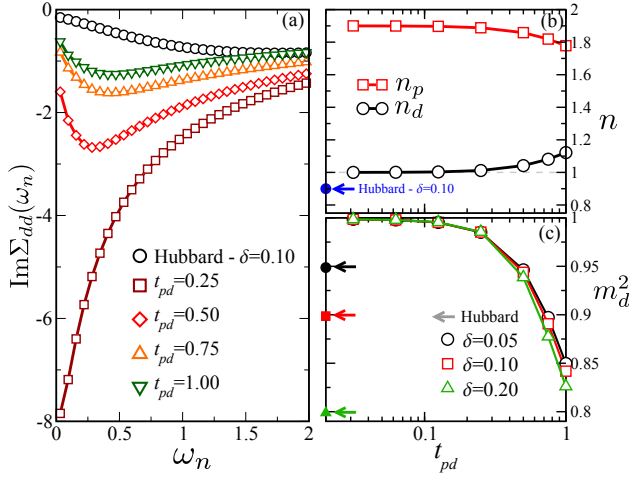


Figure 2. (Color online) (a) Imaginary part of the Matsubara d -electron self-energy $\text{Im}\Sigma_{dd}$ for increasing hybridization amplitude t_{pd} and doping $\delta = 0.10$. (b) p - and d -orbital densities, $\langle n_p \rangle$ and $\langle n_d \rangle$ respectively, as a function of t_{pd} . The arrow to filled symbol indicates $\langle n_d \rangle$ for the Hubbard model with doping $\delta = 0.10$. (c) d -electron local moment $m_d^2 = \langle \hat{S}_z^{(d)2} \rangle$ as a function of t_{pd} and different values of the doping δ . The arrows indicate the Hubbard model results at the same values of δ .

be able to compare solutions with both finite t_{pd} and finite doping to a *doped* Hubbard model. However, we can not recover the latter in the limit of vanishing t_{pd} of our model, as this tends towards a *half-filled*, “ d -only” Mott insulator. Hence, we shall complement our calculations by solving the Hubbard model for a given (in principle arbitrary) value of the hole-doping δ . We will fix δ according to physically motivated criteria, *e.g.* that the size of the instantaneous spin moment is that of the solution with finite t_{pd} we are comparing to, or, that the occupation of the d -orbital $\langle n_d \rangle$ is the same between the two models.

In order to place the system into the “charge-transfer” regime we consider the model defined in Eq. (1) with $U = 3.5$ and $\Delta = -0.5$. In addition we set the temperature to $T = 1/100$.

The existence of two different screening channels of the local moments has a very strong effect on the spin dynamics. This is illustrated in Fig. 1, where results for the local spin susceptibility χ_{spin} (both in ω and in τ) are shown for different values of t_{pd} and total occupation $n = \langle n_d \rangle + \langle n_p \rangle = 2.9$, as well as for the “ d -only” Hubbard model at $\delta = 0.10$. As it can be seen in the inset of Fig. 1 and in Fig. 2c, where we show the d -electrons local moment $m_d^2 = \langle \hat{S}_z^{(d)2} \rangle$, the latter calculation yields the same instantaneous (*i.e.* $\tau = 0$) moment of the case of the t_{dd} -PAM with $t_{pd} = 0.75$.

In order to disentangle the contribution of the screening channels, we shall discuss the behavior of $\chi_{\text{spin}}(\omega)$ of Fig. 1 in more detail. In the “ d -only” Hubbard case the instantaneous local moment is dynamically screened

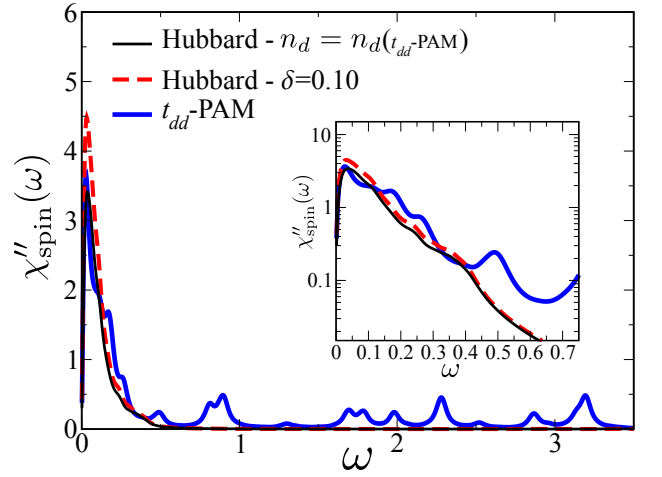


Figure 3. (Color online) Comparison of the spin susceptibility $\chi_{\text{spin}}(\omega)$ of the t_{dd} -PAM with $t_{pd} = 0.75$ and doping $\delta = 0.10$ (thick line) with two “ d -only” Hubbard model calculations (thin and dashed lines). The thin line shows the case with d -electrons occupation $\langle n_d \rangle$ equal to the value of n_d in the t_{dd} -PAM. The dashed line shows the case at fixed doping $\delta = 0.10$. Inset: blow-up of the low-frequency behavior from the main panel.

by coherent metallic excitations at the Fermi level, as indicated by the vanishing imaginary part of the self-energy (see Fig. 2a). In this regime, the screening process is entirely coming from d - d direct exchange with a leading coupling $J_{dd} \simeq \alpha^2 t_{pp}^2 / U$, as the p -electrons are completely decoupled. Correspondingly, the spin susceptibility $\chi_{\text{spin}}(\omega)$ is dominated by low-energy contributions, though weaker high-energy features at $\omega \simeq U$, associated to electronic excitations across the Hubbard bands, can be detected.

If we now consider the extreme case of very large hybridization strength, *i.e.* $t_{pd} = 1$, we notice pronounced changes in the spin susceptibility. First of all the low-frequency part acquires more structures, as further underlined in Fig. 3 where the case $t_{pd} = 0.75$ is directly compared to two “ d -only” solutions: one for $\delta = 0.10$ and the other for the same value of $\langle n_d \rangle$ as in our model. Big differences can be seen in the intermediate-to-high frequency region. The $\chi_{\text{spin}}(\omega)$ of the t_{dd} -PAM acquires there a significant weight and several additional peaks are visible. As highlighted in Fig. 1, these features extend in a frequency range with a width set by the p -electrons bandwidth $2D$, while their position scales with $\sqrt{\Delta^2 + 4t_{pd}^2}$. The latter corresponds to the correction to the charge-transfer energy from hybridized bands repulsion, confirming that the intermediate-to-high lying peaks come from the hybridization with the more delocalized p -orbitals.

We now focus on the low-frequency region, *i.e.* for $\omega < 1$. A blow-up is shown in the inset to Fig. 3. Evidently, the two “ d -only” calculations both display less structures than the t_{dd} -PAM (blue line). This suggests

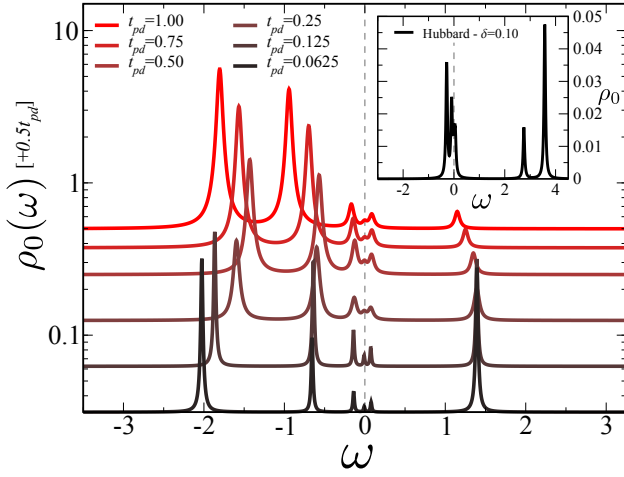


Figure 4. (Color online) Spectral density of the hybridization function $\rho_0(\omega) = -\text{Im}\Delta_{dd}(\omega)/\pi$ for increasing amplitudes t_{pd} . Inset: the same quantity for the “ d -only” Hubbard model.

that the low-frequency feature of the spin susceptibility of the t_{dd} -PAM has a mixed d - p character. In fact, in this region we expect both the d - d screening processes and the d - p ones to be active. To estimate the order of the screening processes one can consider that in the presence of finite hybridization the d -electrons have an effective hopping of the order $t_{\text{eff}} = \alpha t_{pp} + t_{pd}^2/\Delta$. Then, using a simple super-exchange argument, we can associate a number of coupling constants to the different local moments screening processes as follows:

$$J_{dd} \simeq \frac{\alpha^2 t_{pp}^2}{U}, \quad J_{pd}^{(1)} \simeq \frac{2\alpha t_{pp} t_{pd}^2}{\Delta U}, \quad J_{pd}^{(2)} \simeq \frac{t_{pd}^4}{\Delta^2 U}. \quad (4)$$

As pointed out before, the first constant describes direct d - d processes. The other two describe screening processes involving two or four hybridizations with non-interacting electrons and, respectively, one or no direct hopping events. For large values of t_{pd} the $J_{pd}^{(1)}$ dominates at low-energy. On the other hand, for small value of the hybridizations $J_{pd}^{(2)}$ becomes smaller than $J_{pd}^{(1)}$ and the associated exchanges processes dominates at low-frequency.

We can attempt to relate the estimates of Eq. (4) to the structures of $\chi_{\text{spin}}(\omega)$ shown in the inset to Fig. 3. For the parameters used, J_{dd} is the smallest coupling ($\mathcal{O}(10^{-3})$) and it can be associated to the lowest-energy onset of $\chi_{\text{spin}}(\omega)$ present in all three cases. $J_{pd}^{(1)}$ assumes the value of 0.04 which roughly corresponds to the position of the first deviation (dip) between the t_{dd} -PAM curve and the “ d -only” Hubbard solutions. The largest coupling $J_{pd}^{(2)}$ (of the order of 0.4) falls in the region separating the low-energy structures from the intermediate-energy ones, where the largest deviations from the “ d -only” Hubbard start to appear.

In the remaining part of this section we discuss the behaviour of the spin susceptibility as we decrease t_{pd} down to very small values. As shown in Fig. 2b this cor-

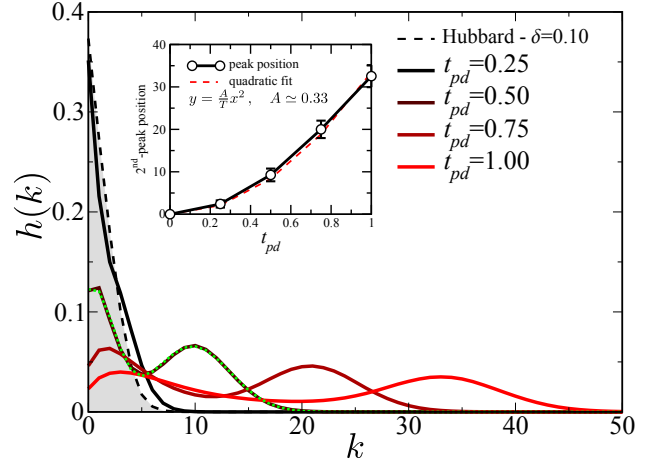


Figure 5. (Color online) Histogram $h(k)$ of the distribution of fermionic diagrams contributing to the local CTQMC trace for different expansion order k . The histograms are shown for different values of the hybridization t_{pd} at fixed doping $\delta = 0.10$. For the Hubbard model case (dashed line) the distribution has one single peak. For the t_{dd} -PAM ($t_{pd} \neq 0$) the curves assume a bi-modal distribution with both “low-order” and “high-order” features. Each of these curves is fitted by a double gaussian (dotted line). Inset: The position of the second peak scales quadratically in t_{pd} . The peak position and error bars are estimated from the mean value and standard deviation of the double gaussian fits.

responds to reducing the mixed valence character of the t_{dd} -PAM solution. As we mentioned above, the occupation $\langle n_d \rangle$ of the d -orbital approaches 1 from above while $\langle n_p \rangle$ saturates to 1.9 in order to keep the total density to 2.9. Concomitantly, the size of the instantaneous moment (see Fig. 2c) increases towards the atomic value of 1. The imaginary part of the self-energy becomes very large at low frequency, reflecting the strong incoherent character of the solution^{31–35} (see Fig. 2a). In this regime of very small t_{pd} the screening is poor. Indeed, the spin susceptibility is very small and essentially featureless. A remnant of the low-frequency peak can still be detected for $t_{pd} = 0.125$ and a structure related to the excitations between the lower Hubbard band and the (suppressed) spectral density at the Fermi level, is recognizable at energies of order U .

IV. DIAGRAMMATIC CHARACTERIZATION

The previous analysis revealed the existence of a number of new features in the spin susceptibility which are an inevitable consequence of the inclusion of p -electrons. Yet, χ_{spin} is not the ideal physical quantity to understand whether or not the new hybridization processes come entirely from p degrees of freedom. In this section we introduce a quantity which turns out to be able to discriminate between d and p character of the hybridization processes

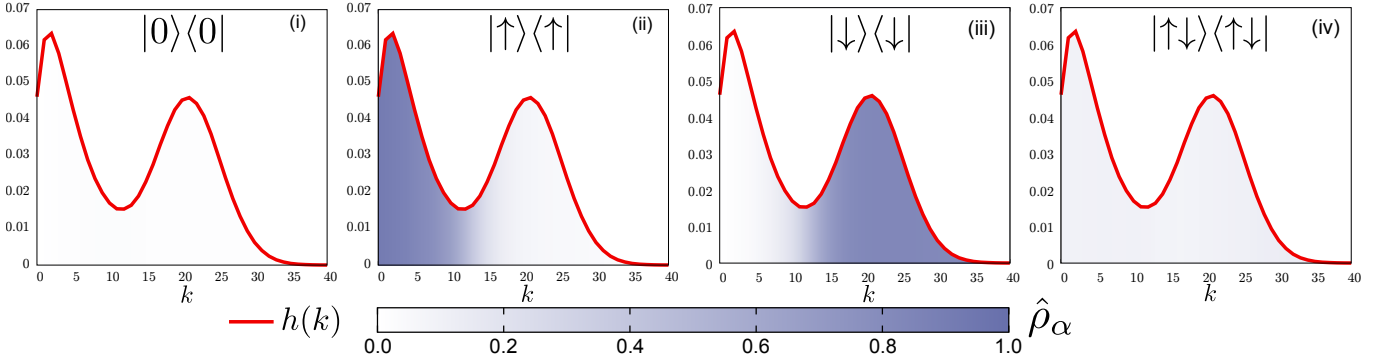


Figure 6. (Color online) State-resolved density-matrix contribution to the expansion order histogram (see text). Data are for the t_{dd} -PAM with $t_{pd}=0.75$, $\delta=0.10$ and bath spin-state $\sigma=\uparrow$. The states of $\hat{\rho}_\alpha$ in different panels are $|0\rangle\langle 0|$ (i), $|\uparrow\rangle\langle\uparrow|$ (ii), $|\downarrow\rangle\langle\downarrow|$ (iii), $|\uparrow\downarrow\rangle\langle\uparrow\downarrow|$ (iv). The figure shows the different contribution to the trace coming from the possible states configuration. The empty and doubly occupied states do not contribute much to the trace. The only significant contribution comes from the singly occupied states and interestingly the two peaks have complementary character.

To begin with, we consider the hybridization function $\Delta_{dd}(\omega) = \sum_{l=1}^{N_b} V_l^2 / (\omega^+ - \epsilon_l)$ on the real-frequency axis. This contains essential information about the formation of electronic excitations involved in the screening channel. Then, using this discretized hybridization function, we perform strong-coupling CTQMC calculations in order to “visualize” distinct classes of diagrams responsible for the different screening effects.

In Fig. 4 we show the spectral density of the hybridization function $\rho_0(\omega) = -\text{Im}\Delta_{dd}(\omega)/\pi$ for several values of t_{pd} and finite doping. For the Hubbard model (see inset) this quantity has a finite weight at the Fermi level, separated by higher energy feature describing hybridization events with doubly occupied states (Hubbard band). For our model at tiny values of t_{pd} $\rho_0(\omega)$ shows a dramatic reduction of the weight at Fermi level, in agreement with the loss of coherence of this metallic state. It is very clear how increasing t_{pd} drives the formation of substantial spectral weight below and at the Fermi level. Therefore the system gains a lot of kinetic energy by introducing hybridization events in that frequency region.

We now turn our attention to the effects introduced by these “new” hybridization events, from a diagrammatic point of view. In Fig. 5 we show the fraction of diagrams contributing to the fermionic trace in the CTQMC calculation as a function of the expansion order, *i.e.* the histogram $h(k)$ of the order of the diagrams involved in the calculation. The histogram of the “ d -only” Hubbard model corresponds to a single contribution near zero-order. For the t_{dd} -PAM the low-expansion order feature gets instead less pronounced and, interestingly, a second structure develops at larger expansion orders. How can we understand this new higher-order peak and can we assign a “label” to it?

A first hint that the second peak at higher expansion orders reflects the presence of the p -orbital comes from the t_{pd} dependence of its position. The expansion order histograms are very well fitted by a double gaussian

function. The mean value of the high-order feature scales quadratically with t_{pd} (see inset of Fig. 5).

A more quantitative label is however needed. This is obtained by looking at the orbital, spin and expansion order resolved site-reduced density matrix which can be directly measured within the CTQMC calculation. The density matrix itself, whose diagonals are the state weights^{36,37}, is defined as $\hat{\rho}_\alpha = |\alpha\rangle\langle\alpha|$ where $|\alpha\rangle$ is an atomic many-body state of the local part of the impurity Hamiltonian. In the present, simple, case of density-density interaction we have $|\alpha\rangle = |0\rangle, |\uparrow\rangle, |\downarrow\rangle, |\uparrow\downarrow\rangle$ and only the state weights are non-zero. The density-matrix $\hat{\rho}_\alpha$ was previously used in similar contexts, *e.g.* Ref. 38, to obtain information about how much time the system spends in a given local state. By resolving its measurement also in the expansion order, this quantity tells us the probability to find the system in a certain atomic state when there are a specific number of hybridization events with a given spin and orbital state.

With this piece of information we can assign an expansion-order dependent intensity to each histogram of Fig. 5. In other words we look at the expansion order for a certain spin and orbital and show as color intensity the value of the state weight for a fixed atomic state at each expansion order. In Fig. 6 we show this quantity for the case of $t_{pd}=0.75$. This unveils a very interesting property of the hybridization-expansion CTQMC histogram for the t_{dd} -PAM with finite hybridization.

In the Hubbard model case the order-resolved density matrix does not display a particularly strong expansion-order dependence. Therefore plotting the histogram with the colors from the density matrix would not be particularly revealing. Instead, in the case of the t_{dd} -PAM the two peaks in the histogram are characterized by almost completely separated classes of diagrams, as indicated by the complementary color intensities in panels (ii) and (iii) of Fig. 6. The density matrix used for the colors of Fig. 6 is calculated for a fixed number k of pairs of oper-

ators with spin $\sigma = \uparrow$ in the local trace. Panel (iii) showing $\hat{\rho}_{\downarrow}$ therefore tells us that a large number of diagrams with many (*i.e.* high expansion-order) spin- \uparrow electrons hopping from and to the impurity contribute to a measure of the local state $|\downarrow\rangle$. This means that the impurity often visits the state $|\uparrow\downarrow\rangle$, *i.e.* the hybridization with the bath makes it often doubly occupied. Since t_{pd} is large and the p -band is almost filled ($\langle n_p \rangle \simeq 1.8$ electrons), the p -orbital acts as a very efficient particle-donor with respect to the impurity, indicating that the peak at large k describes hybridization processes of mostly p -character. We have checked that in a specular situation, with the p -orbital almost empty, the peak at large k has intense color for ρ_{\uparrow} , *i.e.* it corresponds to diagrams “emptying” the impurity. Since in that case the p -orbital “accepts” electrons the same conclusion of the large- k peak being mostly of p -character holds.

The interpretation of the large- k peak as stemming mainly from the hybridization with the p -orbital suggests the following consideration. Since in the hybridization-expansion CTQMC the mean value of the expansion order histogram is proportional to the kinetic energy²⁸, for $t_{pd} \neq 0$ we can identify the presence of two distinct components in the system, one with smaller kinetic energy predominantly of d -character and a more mobile one of p -character (see Figs.5 and 6). The latter component is characterized by a large expansion order therefore it corresponds to large hybridization strength.

Let us note that we cannot directly relate peaks in the expansion-order histogram to specific frequency structures of $\chi_{\text{spin}}(\omega)$. Nevertheless, the previous analysis of the expansion-order resolved density-matrix allowed us to indirectly relate the presence of the feature at large k , containing contributions to the impurity screening coming from mainly p -electrons, to the d - p character of the spin susceptibility. A more formal connection between the expansion-order histogram and response functions of the impurity model can be established by evaluating higher moments of the distribution. For example the width of the second peak in $h(k)$ can give information about “ p -only” contributions to impurity susceptibilities. The present study provides a basis for such an analysis, which we leave for a future investigation.

V. CONCLUSIONS

In this paper, using DMFT we have investigated a simplified, yet generic, model for d - (or f -) orbital materi-

als, explicitly including hybridization with more itinerant, *e.g.* ligand p -, orbitals. We focused on the paradigmatic example of doped charge-transfer insulators. In particular, we studied the evolution of the dynamical spin response $\chi_{\text{spin}}(\omega)$ as a function of the hybridization. We pointed out the existence of different exchange mechanisms involved in the local moment screening. We showed that the direct exchange between d -orbitals, which characterize the screening physics of Hubbard-like models, competes with indirect exchange mechanisms (Kondo singlet formation) involving hybridization with conduction band electrons. We show how the presence of such different exchange mechanisms is reflected in the structure of the spin susceptibility. The low-frequency feature associated to the metallic screening of local moments of the Hubbard model, acquires a multi-peaked structures containing contributions from both direct and indirect processes in the hybridized system. Moreover, the presence of additional screening channels is mirrored in the dynamical spin response by the formation of spectral weight at intermediate energies, extending over an energy range of the order of the conduction electrons bandwidth. Using CTQMC, we characterized the different processes involved in the dynamical screening of instantaneous local moments in terms of diagrams in the hybridization-expansion around the atomic limit. We show that in the presence of finite hybridization, the expansion-order histogram acquires a characteristic double-peak structure revealing the concomitant presence of a more localized and a more mobile electronic component. A special analysis of the expansion-order state-resolved density matrix allows us to assign a meaning to the peaks in the CTQMC histogram, associating them to d - or p -hybridization events separately. Our approach can be very useful in realistic calculations for quantifying the relative importance and the degree of intertwinement of the different screening channels of local moments in materials with orbitals of different degree of localization such, *e.g.* metallic cobaltates³⁸.

Acknowledgments. We acknowledge useful discussions with S. Ciuchi, L. de’ Medici, V. Hinkov, J. Kuneš and A. Toschi. G.S. acknowledges support by the Deutsche Forschungsgemeinschaft (FOR 1162). A.A. and M.C. acknowledge financial support from the European Research Council under FP7 Starting Independent Research Grant n.240524 “SUPERBAD”.

¹ Luuk J.P. Ament, M. van Veenendaal, T.P. Devereaux, J.P. Hill, and J. van den Brink, “Resonant inelastic x-ray scattering studies of elementary excitations,” *Rev. Mod. Phys.* **83**, 705–767 (2011).

² L. Braicovich, J. van den Brink, V. Bisogni, M. Moretti Sala, L. J. P. Ament, N. B. Brookes, G. M. De Luca,

M. Salluzzo, T. Schmitt, V. N. Strocov, and G. Ghiringhelli, “Magnetic Excitations and Phase Separation in the Underdoped $\text{La}_{1-x}\text{Sr}_x\text{CuO}_4$ Superconductor Measured by Resonant Inelastic X-Ray Scattering,” *Phys. Rev. Lett.* **104**, 077002 (2010).

- ³ M. Le Tacon, G. Ghiringhelli, J. Chaloupka, M. Moretti Sala, V. Hinkov, M. W. Haverkort, M. Minola, M. Bakr, K. J. Zhou, S. Blanco-Canosa, C. Monney, Y. T. Song, G. L. Sun, C. T. Lin, G. M. De Luca, M. Salluzzo, G. Khaliullin, T. Schmitt, L. Braicovich, and B. Keimer, "Intense paramagnon excitations in a large family of high-temperature superconductors," *Nat. Phys.* **7**, 725–730 (2011).
- ⁴ T. Kroll, M. Knupfer, J. Geck, C. Hess, T. Schwieger, G. Krabbes, C. Sekar, D. R. Batchelor, H. Berger, and B. Büchner, "X-ray absorption spectroscopy of Na_xCoO_2 layered cobaltates," *Phys. Rev. B* **74**, 115123 (2006).
- ⁵ G. Lang, J. Bobroff, H. Alloul, G. Collin, and N. Blanchard, "Spin correlations and cobalt charge states: Phase diagram of sodium cobaltates," *Phys. Rev. B* **78**, 155116 (2008).
- ⁶ S. Chi, A. Schneidewind, J. Zhao, L.W. Harriger, L. Li, Y. Luo, G. Cao, Z. Xu, M. Loewenhaupt, J. Hu, and P. Dai, "Inelastic Neutron-Scattering Measurements of a Three-Dimensional Spin Resonance in the FeAs-Based $\text{BaFe}_{1.9}\text{Ni}_{0.1}\text{As}_2$ Superconductor," *Phys. Rev. Lett.* **102**, 107006 (2009).
- ⁷ M. Liu, L.W. Harriger, H. Luo, M. Wang, R.A. Ewings, T. Guidi, H. Park, K. Haule, G. Kotliar, S.M. Hayden, and P. Dai, "Nature of magnetic excitations in superconducting $\text{BaFe}_{1.9}\text{Ni}_{0.1}\text{As}_2$," *Nat. Phys.* **8**, 376–381 (2012).
- ⁸ K.-J. Zhou, Y.-B. Huang, C. Monney, X. Dai, V. N. Strocov, N.-L. Wang, Z.-G. Chen, C. Zhang, P. Dai, L. Patthey, J. van den Brink, H. Ding, and T. Schmitt, "Persistent high-energy spin excitations in iron-pnictide superconductors," *Nat. Commun.* **4**, 1470 (2013).
- ⁹ C. Raas, P. Grete, and G. Uhrig, "Emergent Collective Modes and Kinks in Electronic Dispersions," *Phys. Rev. Lett.* **102**, 076406 (2009).
- ¹⁰ P. Grete, S. Schmitt, C. Raas, F.B. Anders, and G. Uhrig, "Kinks in the electronic dispersion of the Hubbard model away from half filling," *Phys. Rev. B* **84**, 205104 (2011).
- ¹¹ P. Hansmann, R. Arita, A. Toschi, S. Sakai, G. Sangiovanni, and K. Held, "Dichotomy between Large Local and Small Ordered Magnetic Moments in Iron-Based Superconductors," *Phys. Rev. Lett.* **104**, 197002 (2010).
- ¹² A. Toschi, R. Arita, P. Hansmann, G. Sangiovanni, K. Held, and a. Toschi, "Quantum dynamical screening of the local magnetic moment in Fe-based superconductors," *Physical Review B* **86**, 64411 (2012).
- ¹³ Masatoshi Imada, Atsushi Fujimori, and Yoshinori Tokura, "Metal-insulator transitions," *Rev. Mod. Phys.* **70**, 1039–1263 (1998).
- ¹⁴ A. Georges, W. Krauth, G. Kotliar, and M.J. J Rozenberg, "Dynamical mean-field theory of strongly correlated fermion systems and the limit of infinite dimensions," *Rev. Mod. Phys.* **68**, 13 (1996).
- ¹⁵ L. de' Medici, A. Georges, G. Kotliar, and S. Biermann, "Mott Transition and Kondo Screening in f-Electron Metals," *Phys. Rev. Lett.* **95**, 066402 (2005).
- ¹⁶ M. Jarrell, H. Akhlaghpour, and T. Pruschke, "Periodic Anderson model in infinite dimensions," *Phys. Rev. Lett.* **70**, 1670–1673 (1993).
- ¹⁷ M. Jarrell, "Symmetric periodic Anderson model in infinite dimensions," *Phys. Rev. B* **51**, 7429–7440 (1995).
- ¹⁸ T. Pruschke, R. Bulla, and M. Jarrell, "Low-energy scale of the periodic Anderson model," *Phys. Rev. B* **61**, 799–809 (2000).
- ¹⁹ G. Sordi, A. Amaricci, and M.J. Rozenberg, "Metal-Insulator Transitions in the Periodic Anderson Model," *Phys. Rev. Lett.* **99**, 196403 (2007).
- ²⁰ F. Lechermann, A. Georges, A. Poteryaev, S. Biermann, M. Posternak, A. Yamasaki, and O. K. Andersen, "Dynamical mean-field theory using Wannier functions: A flexible route to electronic structure calculations of strongly correlated materials," *Phys. Rev. B* **74**, 125120 (2006).
- ²¹ M. J. Han, Xin Wang, C. A. Marianetti, and A. J. Millis, "Dynamical Mean-Field Theory of Nickelate Superlattices," *Phys. Rev. Lett.* **107**, 206804 (2011).
- ²² N. Parragh, G. Sangiovanni, P. Hansmann, S. Hummel, K. Held, and A. Toschi, "Effective crystal field and Fermi surface topology: a comparison of d- and dp-orbital models," *arXiv:1303.2099* (2013).
- ²³ K. Haule, T. Birol, and G. Kotliar, "Covalency in transition metal oxides within all-electron Dynamical Mean Field Theory," *arXiv:1310.1158* (2013).
- ²⁴ M. Caffarel and W. Krauth, "Exact diagonalization approach to correlated fermions in infinite dimensions: Mott transition and superconductivity," *Phys. Rev. Lett.* **72**, 1545–1548 (1994).
- ²⁵ M. Capone, L. de' Medici, and A. Georges, "Solving the dynamical mean-field theory at very low temperatures using the Lanczos exact diagonalization," *Phys. Rev. B* **76**, 245116 (2007).
- ²⁶ C. Weber, A. Amaricci, M. Capone, and P.B. Littlewood, "Augmented hybrid exact-diagonalization solver for dynamical mean field theory," *Phys. Rev. B* **86**, 1–5 (2012).
- ²⁷ P. Werner, A. Comanac, L. de' Medici, M. Troyer, and A. J. Millis, "Continuous-Time Solver for Quantum Impurity Models," *Phys. Rev. Lett.* **97**, 76405 (2006).
- ²⁸ K. Haule, "Quantum Monte Carlo impurity solver for cluster dynamical mean-field theory and electronic structure calculations with adjustable cluster base," *Phys. Rev. B* **75**, 155113 (2007).
- ²⁹ A. M. Läuchli and P. Werner, "Krylov implementation of the hybridization expansion impurity solver and application to 5-orbital models," *Phys. Rev. B* **80**, 1–8 (2009).
- ³⁰ N. Parragh, A. Toschi, K. Held, and G. Sangiovanni, "Conserved quantities of SU(2)-invariant interactions for correlated fermions and the advantages for quantum Monte Carlo simulations," *Phys. Rev. B* **86**, 155158 (2012).
- ³¹ A.N. Tahvildar-Zadeh, M. Jarrell, and J.K. Freericks, "Protracted screening in the periodic Anderson model," *Phys. Rev. B* **55**, R3332–R3335 (1997).
- ³² S. Burdin, A. Georges, and D. Grempel, "Coherence Scale of the Kondo Lattice," *Phys. Rev. Lett.* **85**, 1048–1051 (2000).
- ³³ S. Burdin and V. Zlatić, "Multiple temperature scales of the periodic Anderson model: Slave boson approach," *Phys. Rev. B* **79**, 115139 (2009).
- ³⁴ A. Amaricci, G. Sordi, and M.J. Rozenberg, "Non-Fermi-Liquid Behavior in the Periodic Anderson Model," *Phys. Rev. Lett.* **101**, 1–4 (2008).
- ³⁵ A. Amaricci, L. de' Medici, G. Sordi, M. J Rozenberg, and M. Capone, "Path to poor coherence in the periodic Anderson model from Mott physics and hybridization," *Phys. Rev. B* **85**, 235110 (2012).
- ³⁶ Philipp Werner and Andrew J. Millis, "Hybridization expansion impurity solver: General formulation and application to Kondo lattice and two-orbital models," *Phys. Rev. B* **74**, 155107 (2006).

- ³⁷ P. Werner and A. J.J. Millis, “High-Spin to Low-Spin and Orbital Polarization Transitions in Multiorbital Mott Systems,” *Phys. Rev. Lett.* **99**, 126405 (2007).
- ³⁸ J. Kuneš, V. Křápek, N. Parragh, G. Sangiovanni, A. Toschi, and A. V. Kozhevnikov, “Spin State of Negative Charge-Transfer Material SrCoO_3 ,” *Phys. Rev. Lett.* **109**, 117206 (2012).